STUDIA INFORMATICA 2005
Volume 26 Number 1 (62)

Katarzyna STĄPOR, Adam ŚWITOŃSKI
Politechnika Śląska, Instytut Informatyki

AUTOMATIC DETECTION OF EXUDATES FROM FUNDUS EYE IMAGES BASED ON MATHEMATICAL MORPHOLOGY FOR DIABETIC RETINOPATHY MONITORING

Summary. In this paper the method for automatic segmentation of exudates from fundus eye images is proposed. The method is composed of the following steps: 1) preprocessing, 2) finding marker image and 3) geodesic reconstruction. The mean sensitivity is 95%.

Keywords: mathematical morphology, geodesic reconstruction, exudates, diabetic retinopathy

AUTOMATYCZNA DETEKCJA WYSIĘKÓW NA CYFROWYCH OBRAZACH DNA OKA ZA POMOCĄ METOD MORFOLOGII MATEMATYCZNEJ DLA MONITOROWANIA RETINOPATII CUKRZYCOWEJ

Streszczenie. W artykule przedstawiono metodę segmentacji wysięków na cyfrowych obrazach dna oka. Metoda składa się z następujących kroków: 1) przetwarzanie wstępne, 2) znajdowanie obrazu znaczników, 3) rekonstrukcja geodezyjna. Średnia czułość metody wynosi 95%.

Słowa kluczowe: morfologia matematyczna, rekonstrukcja geodezyjna, wysięki, retinopatia cukrzycowa

1. Introduction

Background *diabetic retinopathy* is a severe and widely spread eye disease. It is the commonest cause of blindness in the current population. At its initial stage, the disease stays in the background, with no symptoms. As a result, the patient is oblivious of its presence. At

this point, there is not an immediate threat of vision impairment, but it is the beginning of serious damage to the retina and it is considered to be the first stage of blood vessel deterioration.

The characteristic features of background retinopathy are microaneurysms, hemorrhages and exudates [2].

Diabetic retinopathy can be treated by laser surgery, in which a strong light beam is aimed on to the retina to shrink the abnormal vessels. Laser surgery has been proved to reduce the risk of severe vision loss from background diabetic retinopathy by 90%.

The most dangerous threats to vision in diabetes give little or no warning. Therefore, regular retinal examinations of the risk groups are highly recommended. The costs of these examinations and the shortage of specialists, especially in rural areas, are the drawbacks of this procedure. Furthermore, in order to monitor the disease, comparison between the images taken at different examinations is necessary. Up to now, the number of lesions (microaneurysms, exudates) is compared, but it would lead to a more sophisticated diagnosis, if one could compare the evolution of each single lesion. Because this task can hardly be fulfilled manually, a computer assisted approach is required – consisting of detecting lesions in retinal images.

For the above reasons, we think that relying on robust and fast algorithms for detecting lesions of diabetic retinopathy is a crucial point of any computer assistance for the diagnosis of this disease.

This article presents the method for automatic detection of **exudates** from ordinary, color **fundus eye images** (**fei**).

In [8] a semi-automatic method consisting of shade-correction, contrast enhancement, sharpening and manually selected threshold by the user is presented to solve this problem.

In [4] a fully automated algorithm based on image sharpening, shade correction and a combination of local and global thresholding has been proposed.

In [3] algorithm is based on fuzzy c-means clustering and classification by neural network. Preprocessing step consists of color normalization and local contrast enhancement. This works well, but it strongly relies on the local contrast enhancement [5], which amplifies the noise, especially in regions with no features.

Because the results obtained by the existing algorithms for exudates detection are not fully satisfactory, we decided to devise a our method for exudates detection from ordinary, color fei. Similarly like in [7], it is based on the geodesic reconstruction of approximated area of exudates from their backgrounds. We proposed a new method for approximating exudates and additionally a preprocessing step. With those modifications we obtained better results for our images.

2. Basic morphological operators

2.1. Gray-level morphology

In this section we briefly define the basic morphological operators used in this paper (for a comprehensive presentation see [6]). Let D_f and D_B be subsets of Z^2 and $T=\{t_{min}, \ldots, t_{max}\}$ an ordered set of gray levels. A *gray-level image f* can be defined as a function:

$$f : D_f \subset Z^2 \to T$$

Furthermore, we define another image known as a *structuring element B*:

$$B : D_B \subset Z^2 \to T$$

We will restrict to flat, symmetric structuring elements B [6] and assume that point $(0,0) \in D_B$. We can now write the four basic morphological operators: *erosion*, *dilation*, *opening* and *closing* as:

$$E^B(f)(x,y) = \inf_{(j,k)\in D_B}\{f(x-j,y-k)\} \qquad D^B(f)(x,y) = \sup_{(j,k)\in D_B}\{f(x-j,y-k)\}$$

$$O^B(f)(x,y) = D^B(E^B(f)(x,y)) \qquad C^B(f)(x,y) = E^B(D^B(f)(x,y))$$

Symmetric, *morphological gradient* of an image f can be defined as:

$$grad(f)(x,y) = D^B(f)(x,y) - E^B(f)(x,y)$$

Furthermore, we shall define geodesic transformation of an image f: *geodesic erosion* and *dilation* of size n:

$$E^{B,g}_{c(n)}(f)(x,y) = E^{B,g}_{c(1)}(E^{B,g}_{c(n-1)}(f))(x,y) \qquad E^{B,g}_{c(1)}(f)(x,y) = \sup\{E^B(f)(x,y), g(x,y)\}$$

$$D^{B,g}_{c(n)}(f)(x,y) = D^{B,g}_{c(1)}(D^{B,g}_{c(n-1)}(f))(x,y) \qquad D^{B,g}_{c(1)}(f)(x,y) = \inf\{D^B(f)(x,y), g(x,y)\}$$

reconstruction by dilation and *reconstruction by erosion*:

$$R^{B,f}(g)(x,y) = D^{B,g}_{c(\infty)}(f)(x,y) \qquad R^{B,f}_{*}(g)(x,y) = E^{B,g}_{c(\infty)}(f)(x,y),$$

where $D^{B,g}_{c(\infty)}$ ($E^{B,g}_{c(\infty)}$) is the limit, which is obtained by iterating unit geodesic erosion of f above g until stability is reached, i.e.: $D^{B,g}_{c(i)}(f)(x,y) = D^{B,g}_{c(i+1)}(x,y)$

2.2. Binary morphology

In binary morphology ($T=\{0,1\}$) a *binary image* is sometimes defined as a subset F of a set D_f composed of those elements of Z^2 for which the function f has nonzero values:

$$F = \{x \in D_f : f(x) = 1\}$$

Thus, **binary images** are treated as **sets** in a coordinate system. We shall define a *translation operation* of a set F by a vector h as:

$$F_h = F + h = \{x + h : x \in F\}$$

We can now write the four basic binary morphological operators: *erosion, dilation*, *opening* and *closing* as:

$$e^B(F) = \bigcap_{h \in B} F + h \qquad d^B(F) = \bigcup_{h \in B} F + h$$

$$o^B(F) = d^B(e^B(F)) \quad c^B(F) = e^B(d^B(F))$$

We use the similar notation as for gray-level morphology but with lower-case letters in corresponding transformations.

Furthermore, we shall define binary, geodesic transformation of an image F under conditional image (mask) g: *geodesic erosion* and *dilation* of size n:

$$e^{B,g}_{c(n)}(F) = e^{B,g}_{c(1)}(e^{B,g}_{c(n-1)}(F)) \qquad e^{B,g}_{c(1)}(F) = e^B(F) \cup g$$

$$d^{B,g}_{c(n)}(F) = d^{B,g}_{c(1)}(d^{B,g}_{c(n-1)}(F)) \qquad d^{B,g}_{c(1)}(F) = d^B(F) \cap g$$

binary reconstruction by dilation and *reconstruction by erosion*:

$$r^{B,F}(g) = d^{B,g}_{c(\infty)}(F) \qquad r^{B,F}_*(g) = e^{B,g}_{c(\infty)}(F),$$

where $d^{B,g}_{c(\infty)}$ ($e^{B,g}_{c(\infty)}$) is the limit which is obtained by iterating unit geodesic erosion of f above g until stability is reached, i.e.: $d^{B,g}_{c(i)}(F) = d^{B,g}_{c(i+1)}$.

We shall define *binary close-hole* operator which is based on geodesic reconstruction of image F^c:

$$ch(F) = [r^{B,F^c}(F_\partial)]^c,$$

where marker image F_∂ is the boundary of the image window, F^c is set complement.

3. The proposed segmentation method for exudates

The proposed method is composed of three main steps: 1) preprocessing, 2) finding marker image, 3) geodesic reconstruction, which will be described in the following sections.

Exudates are bright yellowish deposits, mainly situated in the posterior pole of the fundus. They are caused by retinal vascular pathologies. Exudates appear as bright white or yellow areas in color fundus images of the human retina (Fig.1a) and usually they are well contrasted. Their shape is usually irregular. Their sizes vary considerably.

3.1. Preprocessing

Having compared several color spaces, we found that the exudates are most contrasted against the background in the *G* channel of the RGB color space [1] (Fig.1b) - image f_G).

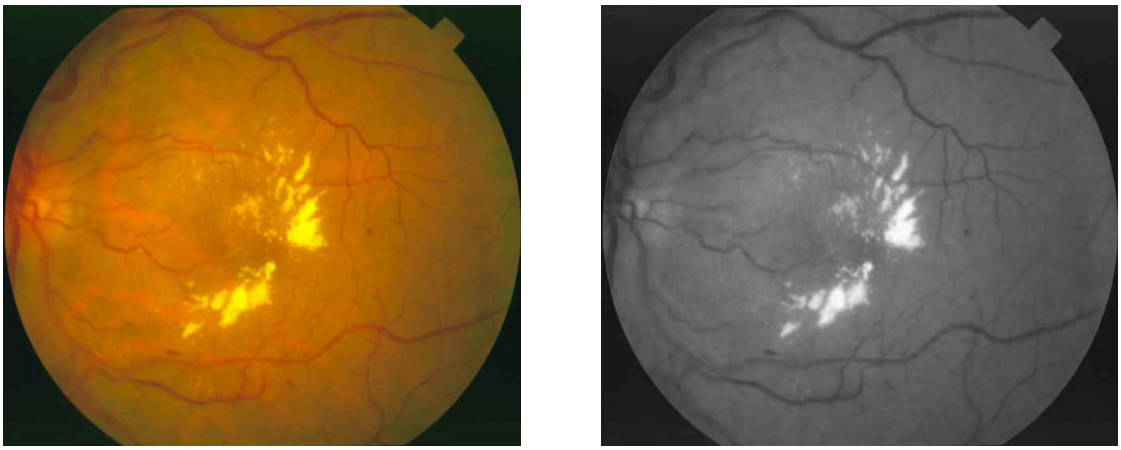

a) b)

Fig. 1. Exudates in fundus eye images: a) color fundus eye image, b) the *G* channel of the input image shown in Fig.1a)

Rys. 1. Wysięki na obrazach dna oka: a) kolorowy obraz dna oka, b) kanał *G* obrazu wejściowego z rys. 1a)

The image f_G is filtered in order to eliminate large gray level variations caused by the outgoing vessels. We "fill" the vessels by applying a simple closing operation:

$$f_G^1 = C^B(f_G)$$

with a structuring element *B* bigger than the maximal width of vessels - we use a circle with a radius 11. The result is shown in Fig.2a).

3.2. Construction of the marker image

Finding the exact contours of the exudates in our method is based on the morphological reconstruction by dilation of the preprocessed image f_G^1 : starting from a properly constructed marker image *g(x)* in the way described below.

First, the approximate contours of the candidate regions are detected by performing the morphological gradient on the filtered image f_G^1 with a structuring element *B* being a *11x11* square:

$$f_G^2 = grad(f_G^1) = D^B(f_G^1) - E^B(f_G^1)$$

We would like to detect all possible contours of exudates, which in some cases are sharp and in others not, but in all of them they reflect a noticeable difference in grayscale values. That's why we decided to use such a large structuring element. It can sometimes cause

detection of extra non exudate contours and in most cases will produce wider contours than they are in fact. Those effects will be minimized and in practice almost always removed by geodesic reconstruction processed in one of the following steps.

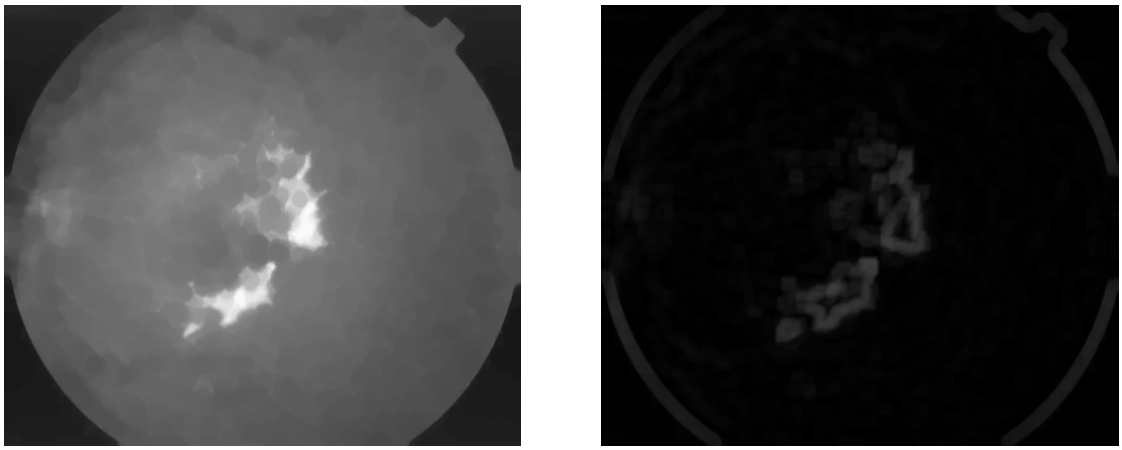

a) b)

Fig. 2. Filtering and contours approximation: a) channel *G* from Fig.1b) after closing operation (image f_G^1), b) gradient of the image f_G^1 (image f_G^2)

Rys. 2. Filtracja i oszacowanie konturów: a) kanał *G* obrazu z rys. 1b) po operacji zamknięcia (obraz f_G^1), b) gradient obrazu f_G^1 (obraz f_G^2)

In the next step a simple thresholding operation is applied to the resulted image f_G^2 to point possible exudates location unambiguously:

$$f_G^3 = T_{T1}(f_G^2)$$

where the global threshold *T1* has been set experimentally (*15* in our case).

Next we "fill" holes in candidate regions detected in the previous step, using the binary close-hole operation which fills in all holes in a binary image that do not touch the image window boundary:

$$f_G^4 = ch^B(f_G^3)$$

The structuring element *B* is *3x3* square.

The marker image g(x) is obtained in the following way:

$$g(x) = \begin{cases} 0 & if \quad x \in f_G^4 \\ f_G^1 & if \quad x \notin f_G^4 \end{cases}$$

All the pixels in a marker image *g(x)* which are objects (i.e. white) in the image f_G^4 are set to zero (black).

A problem arises: On some images where whole fundus area is surrounded by the black background, the given algorithm will detect closed contour between fundus area and its background. In such a situation close-hole operator will fill whole fundus area which will cause improper detection of possible exudates regions. To avoid it, we proposed using wider

boundary of the image from which reconstruction is processed in close-hole operation. We used boundary of the size 30.

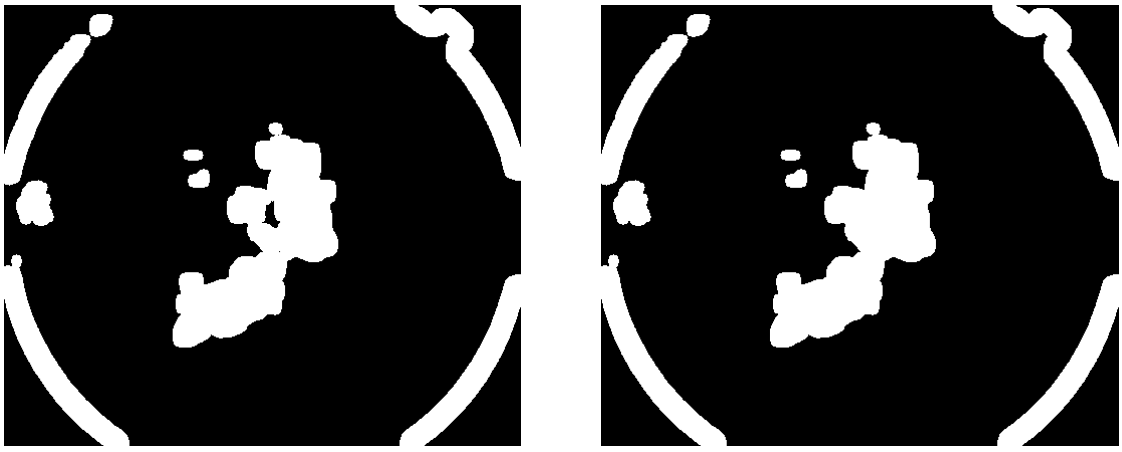

a) b)

Fig. 3. Preliminary detection of exudates: a) gradient image after thresholding (image f_G^3), b) Image f_G^3 after close-hole operation (image f_G^4)

Rys. 3. Wstępna detekcja wysięków: a) obraz gradientowy po operacji progowania (obraz f_G^3), b) obraz f_G^3 po operacji close-hole (obraz f_G^4)

3.3. Geodesic reconstruction

Next, we perform the geodesic reconstruction by dilation of the image f_G^1 from the constructed marker image *g(x)* using a structuring element *B* being a *3x3* square*:*

$$f_G^5 = R_D^{B,g}(f_G^1)$$

The reconstruction operator propagates the values of $f_G^1(x)$ of pixels *x* next to the candidate regions into the candidate regions by successive geodesic dilation under the mask f_G^1. As exudates are entirely comprised within the candidate regions, they are completely removed, whereas regions that are not entirely comprised in the candidate regions are nearly entirely reconstructed.

The final result is obtained by simple thresholding operation to the difference between the image f_G^1 and the reconstructed image f_G^5:

$$f_G^6 = T_{T2}(f_G^1 - f_G^5)$$

The threshold *T2* has been experimentally set to *10*.

Contours of the obtained regions being the detected exudates are shown in Fig.5b) imposed on the input image.

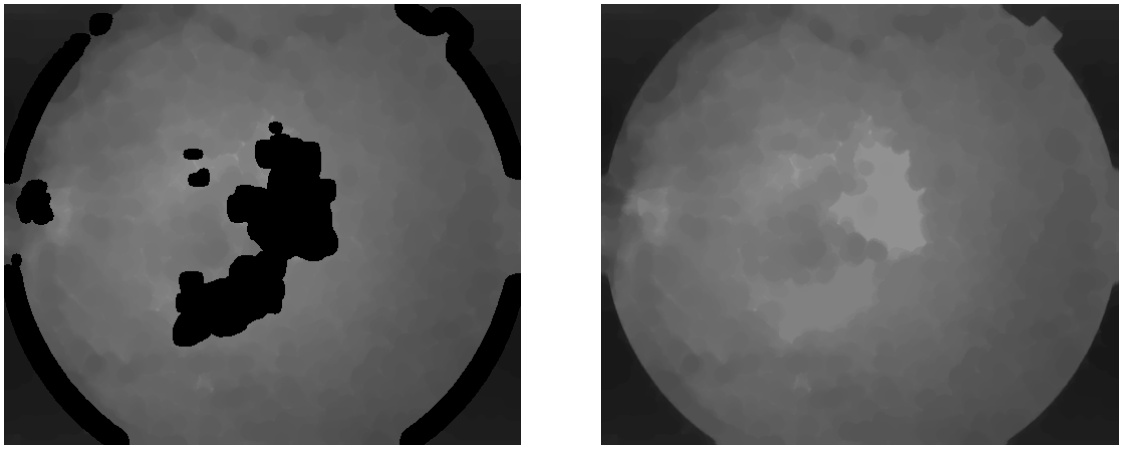

a) b)

Fig. 4. Geodesic reconstruction of approximated area of exudates: a) the marker image g(x), b) the reconstructed image (image f_G^5)

Rys. 4. Rekonstrukcja geodezyjna aproksymowanego obszaru wysięków: a) obraz znaczników g(x), b) obraz po rekonstrukcji (obraz f_G^5)

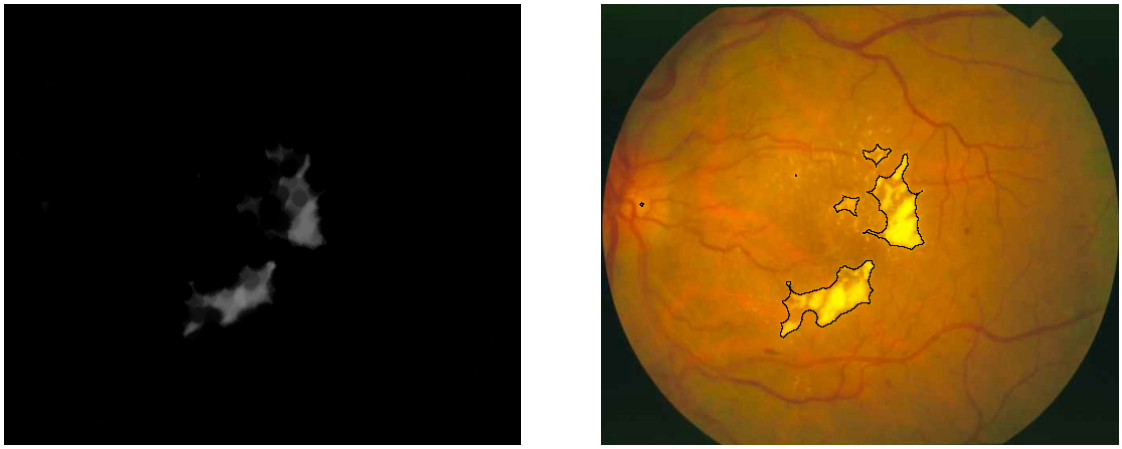

a) b)

Fig. 5. Final results: a) the difference between images f_G^1 and f_G^5, b) the contours of the thresholded image shown in Fig.5a) superimposed on the input image

Rys. 5. Wyniki końcowe: a) różnica między obrazami f_G^1 i f_G^5, b) kontury sprogowanego obrazu z rys. 5a) nałożone na wejściowy obraz

4. Results and conclusions

To evaluate the quality of our algorithm we decided to apply pixelwise method based on the comparison of the results obtained by the algorithm and true exudates. We have tested it on a database of 50 images, which have not been used in the development stage.

We asked a human specialist to mark the exudates on color images. In that way we obtained the manual segmentation result *r1,* which we assumed to be correct. Next we applied our algorithm and obtained result *r2*. We defined *following measures*:

$$sensitivity = \frac{Nr(r2 \cap r1)}{Nr(r1)}$$

$$specificity = \frac{Nr\big(S(r1) \cap S(r2)\big)}{Nr(r1)},$$

where *S(f)* is the support of *f* defined as the set of pixels for which $f(x) \neq 0$, *Nr(S)* is the number of its elements and operator \ is the set difference.

Because of the manual way of marking true exudates by a human grader, which produces a lots of errors near the edges of exudates, we decided not to compare those pixels Similarly like in [7] we applied binary dilation for the resulted image r2. Sensitivity and specificity with that modification are defined as follows:

$$sensitivity = \frac{Nr(D(r2, B) \cap r1)}{Nr(r1)}$$

$$specificity = \frac{Nr\big(S(r1) \cap D(S(r2), B)\big)}{Nr(r1)}$$

We used structuring element B 7x7.

Mean sensitivity was 95% and a specificity 93.2%. Better sensitivity is probably the result of closing operation applied in the first preprocessing stage.

The results are encouraging and we are planning to undertake clinical evaluation in order to integrate the presented algorithm with a tool for diagnosis of diabetic retinopathy.

REFERENCES

1. Gonzalez R. C, Woods R. E: Digital Image Processing. Prentice-Hall, 2002.
2. Kanski J. et al.: Clinical ophthalmology. Butterworth-Heinemann, 1996.
3. Osaresh A. et al: Automatic recognition of exudative maculopathy using fuzzy c-means clustering and neural networks. Proc. Medical Image Understanding and Analysis Conference, 2001, 49-52.
4. Philips R. et al: Automated detection and quantification of retinal exudates. Graefe's Archive for Clinical and Experimental Opthalmology, v.231, 1993, 90-94.
5. Sinthanayothin C. et al: Automated localisation of the optic disc, fovea and retinal blood vessels from digital color fundus images. British Journal of Ophthalmology, v. 83, Nr 8, 1999, 902-910.

6. Soille P.: Morphological Image analysis: principles and applications. Springer-Verlag, Berlin, 1999.
7. Walter T., Klein J. C., Massin P., Erginay A.: A contribution of Image processing to the diagnosis of diabetic retinopathy detection of exudates in color fundus images of the human retina. IEEE Transactions on Medical Imaging, 2002, vol. 21, no 10, s. 1236-43.
8. Ward N.et al: Image analysis of fundus photographs – the detection and measurement of exudates associated with diabetic retinopathy. Ophthalmology, v. 96, 1989, 80-86.

Recenzent: Dr inż. Damian Bereska

Wpłynęło do Redakcji 31 marca 2004 r.

Omówienie

W artykule przedstawiono nową metodę automatycznej segmentacji wysięków na kolorowych, cyfrowych obrazach dna oka pozyskanych z funduskamery. Zaproponowana metoda składa się z następujących kroków: 1) przetwarzanie wstępne, 2) konstrukcja obrazu znaczników, 3) rekonstrukcja geodezyjna. Wszystkie kroki metody wykorzystują transformacje morfologii matematycznej [6]. Automatyczna konstrukcja obrazu znaczników dla rekonstrukcji geodezyjnej bazuje na obrazie gradientowym. Uzyskana średnia czułość metody wynosi 95%. Opracowany algorytm detekcji wysięków stanowiących jedne z symptomów retinopatii cukrzycowej stanowić może jeden z modułów systemu komputerowego wspomagającego diagnozowanie, jak również monitorowanie tej choroby.

Adresses

Katarzyna STĄPOR: Politechnika Śląska, Instytut Informatyki, ul. Akademicka 16, 44-100 Gliwice, Polska, delta@ivp.iinf.polsl.gliwice.pl .
Adam ŚWITOŃSKI, Politechnika Śląska, Instytut Informatyki, ul. Akademicka 16, 44-100 Gliwice, Polska.